Cellular and Molecular Biology

Qin *et al. Cell. Mol. Biol.*2016, 62 (3): 51-64
ISSN: 1165-158X
doi: 10.14715/cmb/2016.62.3.10

Original Research

Alteration of N-glycoproteins/N-glycosites in human hepatic stellate cells activated with transforming growth factor-β1

Y. Qin[1,2#], Q. Wang[2#], Y. Zhong[2], F. Zhao[2], F. Wu[1], Y. Wang[2], T. Ma[2], C. Liu[1], H. Bian[3], Z. Li[2*]

[1] Department of Cell Biology and Genetics, School of Basic Medical Sciences, Xi'an Jiaotong University Health Science Center, Xi'an, Shaanxi 710061, P.R. China

[2] Laboratory for Functional Glycomics, College of Life Sciences, Northwest University, Xi'an 710069, P. R. China

[3] Cell Engineering Research Centre and Department of Cell Biology, Fourth Military Medical University, Xi'an 710032, P. R. China

Abstract: Proteins N-glycosylation is significantly increased in the activated human hepatic stellate cells (HSCs) stimulated by transforming growth factor-β1 (TGF-β1) compared to the quiescent HSCs according to our previous study. However, little is known about the alteration of N-glycoprotein profiles in the activated HSCs. Profiles of N-glycopeptides / N-glycoproteins / N-glycosites in LX-2 cells, with and without activation by TGF-β1, were identified and compared using hydrazide chemistry enrichment coupled with liquid chromatography - mass spectrometry analysis. Western blot and immunohistochemistry were further used for validation. A total of 103 non-redundant N-glycopeptides, with 107 glycosylation sites from 86 N-glycoproteins, were identified in activated and quiescent LX-2 cells respectively. Among these, 23 proteins were known N-glycoproteins, and 58 were newly identified N-glycoproteins. In addition, 43 proteins (e.g., pigment epithelium-derived factor and clathrin heavy chain 1) were solely identified or up-regulated in the activated LX-2 cells, which participated in focal adhesion and glycosaminoglycan degradation pathways and were involved in interaction clusters of cytoskeletal proteins (e.g., myosin light chains and keratins). The increased expression of glucosamine (N-acetyl)-6-sulfatase and phospholipase C beta 2 and the decreased expression of zinc finger and BTB domain-containing protein 1 were validated in the activated compared to the quiescent LX-2 cells. In conclusion, increased expression of N-glycoproteins and N-glycosites play important roles in cellular contractility, signal transduction, and responses to stimuli in the activated HSCs, which might provide useful information for discovering novel molecular mechanism of HSC activation and therapeutic targets in liver fibrosis.

Key words: Hepatic stellate cell, liver fibrosis, N-glycoprotein, N-glycosylation site.

Introduction

Fibrosis is a common liver disease with significant morbidity and mortality, which results from chronic damage to the liver in conjunction with the accumulation of extracellular matrix (ECM) proteins (1). Activation of hepatic stellate cells (HSCs) is the key event in the process of hepatic fibrosis, by which HSCs acquire contractile, proinflammatory, and fibrogenic properties (2,3). Transforming growth factor-β1 (TGF-β1) is a pro-fibrogenic mediator that can induce HSC activation both in vivo and in vitro (4,5).

Glycosylation is a ubiquitous and essential modification of proteins. As many as 70% of all human proteins are estimated to contain one or more glycan chains (6). Two types of protein glycosylation exist: 1) N-glycosylation to the amide nitrogen of asparagine side chains, and 2) O-glycosylation to the hydroxyl groups of serine and threonine side chains. N-Linked glycoproteins play particularly important roles in various biological processes, such as cell-cell adhesion, bacterial infection, viral attachment, and ligand-receptor binding (7-9). Changes in specific N-linked glycoproteins are associated with disease progression. Identification of these N-linked glycoproteins and their N-glycosites has potential applications in disease diagnosis and prognosis, and the prediction of effective treatments (10,11). It is well known that lots of fibrosis-related proteins are N-glycoproteins or N-glycan binding proteins. Hypoxia up-regulated protein 1 and lysosomal alpha-glucosidase are N-glycosylated (12). Interleukin-1 and tumor necrosis factor-α contribute to the activation of HSC (13), have lectin-like activities (14), and recognize disialylated diantennary N-glycans bearing two Neu5Aca2,3 residues (15), and heparin (16). According to our previous study, proteins N-glycosylation recognized by *Aleuria aurantia* lectin (AAL), *Phaseolus vulgaris* agglutinin E (PHA-E) and Erythrina cristagalli agglutinin (ECA) significantly increased in the activated human HSCs stimulated by TGF-β1 compared to the quiescent HSCs (17). Therefore, N-glycoproteins and their N-glycosylation are closely associated with HSC activation and liver fibrosis.

Along with the rapid improvements and increased use of new technologies involving mass spectrometry in the area of glycoproteomics, N-linked glycoprotein/glycopeptides can be enriched by hydrazide chemistry (18,19), lectin affinity chromatography (20,21), immunoaffinity chromatography (22,23), bonic acid chemistry (24,25), size exclusion chromatography (26,27), electrostatic repulsion hydrophilic interaction chromatography (28,29), and hydrophilic interaction chroma-

Received January 5, 2016; **Accepted** March 15, 2016; **Published** March 20, 2016

*** Corresponding author:** Zheng Li, Laboratory for Functional Glycomics, College of Life Sciences, Northwest University, Xi'an, P. R. China. Email: zhengli@nwu.edu.cn

[#] These authors contributed equally to this work.

Copyright: © 2016 by the C.M.B. Association. All rights reserved.

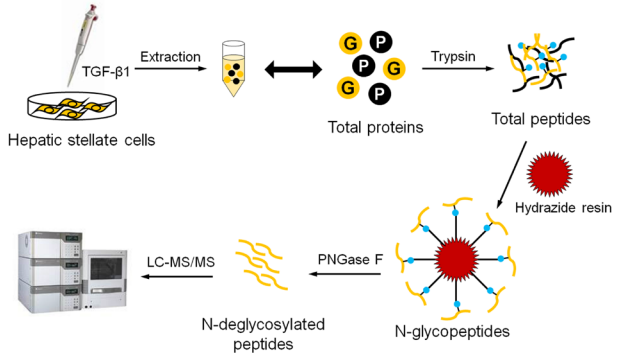

Figure 1. Schematic flow diagram of the integrated strategy used herein.

tography (30). These techniques can be used alone or in combination with others. Hydrazide chemistry is a relatively universal and reliable method for the identification of glycoproteins, as well as glycosylation sites, from complex biological samples. This chemistry is carried out by coupling N-linked glycoproteins to hydrazide resin and then releasing these glycopeptides specifically by digestion with peptide N-glycanase (PNGase). In the current study, hydrazide chemistry enrichment coupled with liquid chromatography-tandem mass spectrometry (LC-MS/MS) identification was used to compare profiles of N-glycoproteins / N-glycopeptides/ and N-glycosites between human HSCs (LX-2 cells) with and without activation by TGF-β1. This integrated strategy is summarized in Fig. 1.

Materials and Methods

Materials

Dulbecco's modified Eagle medium and fetal bovine serum were purchased from Invitrogen (Carlsbad, CA, USA). TGF-β1 was purchased from R&D systems (Minneapolis, MN, USA). AffiGel hydrazide resin was purchased from Bio-Rad (Hercules, CA, USA). Dithiothreitol and iodoacetamide were purchased from GE Healthcare (Waukesha, WI, USA). Urea, NH_4HCO_3, $NaIO_4$, HPLC-grade acetonitrile (ACN), trifluoroacetic acid (TFA), bicinchoninic acid, proteinase inhibitor cocktail, and Bradford assay reagent were purchased from Sigma-Aldrich (St. Louis, MO, USA). Trypsin was purchased from Promega (Madison, WI, USA). PNGase F was purchased from New England Biolabs (Ipswich, MA, USA). Bovine serum albumin was purchased from Merck (Darmstadt, Germany). T-PER reagent was from Pierce Biotechnology (Rockford, IL, USA). Rabbit polyclonal antibodies against glucosamine (N-acetyl)-6-sulfatase (GNS), 1-phosphatidylinositol 4,5-bisphosphate phosphodiesterase beta-2 (PLCB2), and GADPH were from GeneTex Inc. (Irvine, CA, USA). A rabbit polyclonal antibody against zinc finger and BTB domain-containing protein 1 (ZBTB1) was purchased from Abcam Trading Company Ltd. (Shanghai, China). Other chemical reagents were obtained from commercial suppliers and used without further purification.

Amicon Ultra-0.5 3kD devices were obtained from Millipore (Bradford MA, USA). C18 SepPak columns were from Waters (Milford, MA, USA). All solutions were prepared with ultra-pure water obtained from a Milli-Q50 SP Reagent Water System (Millipore). The ZHWY-2101C oscillator was from ZhiCheng Corporation (Suzhou, China). The SpeedVac was from Thermo Scientific (Waltham, MA, USA). HPLC used a Zorbax 300SB C18 analytical column (150 × 0.075 mm, 3.5 mm particles). The Q-TOF 6530 mass spectrometer was from Agilent (Santa Clara, CA, USA).

Cell culture and activation

LX-2 cells were maintained and activated as described previously (17,31). LX-2 cells (2×10^5) were seeded and cultured for 24 h in Dulbecco's modified Eagle high glucose medium supplemented with 10% fetal bovine serum. After 24 h of starvation, cells were activated by adding 2 ng/mL TGF-β1 for an additional 24 h. The control groups were not treated with TGF-β1.

Extraction and trypsin digestion of total protein

Total protein from LX-2 cells was extracted using T-PER reagent as described previously (17,32). Adherent cells were washed twice with ice-cold phosphate buffered saline (PBS) (10 mM sodium phosphate buffer containing 150 mM NaCl, pH 7.4) to remove culture media. Cells were disrupted by repetitive pipetting after a 15 min incubation with 10 µL/mL of T-PER reagent mixed with protease inhibitors. Following centrifugation at 10,000 × *g* for 10 min, the supernatant was collected immediately for use, or stored at −80°C. LX-2 cells were independently treated by three times and the total proteins from each group (n=3) were pooled in order to reduce error. The protein concentration was determined by the bicinchoninic acid assay. Two mg of protein was concentrated at 4°C using a 3 kD Amicon Ultra centrifugal filter with denaturing buffer (8 M urea in 0.1 M NH_4HCO_3 solution, pH 8.3) (33,34) at 12,000 × *g* for 20 min. This was repeated three times with an exchange of solvent to denature the proteins. The proteins were then reduced by incubation for 60 min in 5 mM dithiothreitol at 60°C, and alkylated by 20 mM iodoacetamide at room temperature in the dark for 30 min. The solution was diluted 5-fold with 0.1 M NH_4HCO_3 (pH 8.3) and the proteins were digested overnight with 20 µg sequencing-grade modified trypsin at 37°C. Digestion was terminated by acidifying the sample mixture with TFA to pH < 3. The peptides were desalted by a Sep-Pak® Vac C18 cartridge and eluted in 0.4 mL of 80% ACN/0.1% TFA.

Enrichment of N-glycopeptides by hydrazide chemistry

The N-glycopeptides in LX-2 cells were enriched by hydrazide chemistry as described previously (18,33,34). Briefly, the peptides (~0.5 mg) were oxidized by 10 mM $NaIO_4$ at room temperature for 1 h in the dark. The oxidized peptide samples were diluted 16-fold with 0.1% TFA and purified using a C18 column. The purified peptides were eluted directly into hydrazide resin and incubated overnight at room temperature with shaking. The resin was washed sequentially three times each with 80% ACN, 1.5 M NaCl, and deionized water. The N-linked glycopeptides were released from the resin via 2 µL PNGase F in 100 µl of 25 mM NH_4HCO_3 at 37°C overnight with shaking. The supernatant and wash solutions were combined and lyophilized.

LC-MS/MS analysis

Lyophilized peptides were resuspended in 25 μL of 0.1% formic acid (FA), and 8 μL was used for each LC-MS/MS run. The LC-MS/MS analysis of peptides was conducted using a LC Packing nano-LC system (Agilent 1200 series) with a nanoelectrospray chip interface (Agilent) and a quadrupole TOF mass spectrometer (Agilent 6530 Accurate-Mass QTOF LC/MS). The samples were first loaded onto an HPLC-Chip (G4240-62010, Zorbax 300SB C18 particles) for nano-LC separation at a flow rate of 300 nL/min. The eluents used for the LC were (A) 1% ACN/0.1% FA and (B) 90% ACN/0.1% FA. A gradient was utilized from 3% B to 10% B in 10 min, from 10% B to 45% B in 70 min, from 45% B to 95% B in 10 min, and held at 95% B for 15 min. Then the column was re-equilibrated for 15 min before the next run. Due to the statistical fluctuations of peptide precursor selection during the MS/MS acquisition, two LC-MS/MS assays were run for each sample to facilitate a proper proteome comparison.

Data mining and analysis

Protein identification was accomplished using the MASCOT database search engine (V2.3.02, Matrix Science, London, UK). The MS/MS spectra were used to search the IPI human 3.74 database in which trypsin, and up to two cleavages errors were allowed. The carboxymethylated cysteines (+57 Da) were set as a fixed modification. Oxidized methionine (+16 Da) and deamidization of asparagine (+0.98 Da) were set as variable modifications. A peptide tolerance of 20 ppm and a tolerance of ± 0.7 Da for the fragment ions were used. Glycoproteins were identified from peptides with a Mascot Score above 25 ($p < 0.05$) and a deamidization site on the Sequon motif (asparagine-Xxx-threonine/serine where Xxx should not be proline) ($p < 0.05$). The N-glycopeptides identified were filtered by a deamidated (N) site at the N-X-S/T motif (where X is any amino acid except proline) to reduce potential false positives (35).

Label-free relative quantification of glycoproteins identified by emPAI

The Mascot search engine has incorporated a semi-quantification method, emPAI, which leads to a convenient relative quantification method. To compare activated with quiescent LX-2 cell glycoproteomes, the normalized emPAI value for each protein in each sample for each run was calculated (see Formula 1), and the emPAI values for two runs were averaged and were compared by fold change in the activated versus the quiescent LX-2 cells.

Formula 1: normalized emPAI of a glycoprotein = emPAI of a glycoprotein / sum of all emPAIs in a sample× 100.

Proteome Bioinformatics

Ontology analysis was performed according to the standard Blast2GO procedure (36) to gain insights of the identified N-glycoproteins in three aspects of GO. The differences in GO terms between those of glycoproteins from activated and quiescent LX-2 cells were also determined (37). Biological pathways represented by the identified glycoproteins were from the KEGG human pathway database (38). To validate the results of the Blast2GO and KEGG analyses, an independent functional enrichment analysis was performed using DAVID (Database for Annotation, Visualization and Integrated Discovery) (39). Finally, to assess the functional relevance of the differentially expressed glycoproteins, a protein-protein interactive network analysis was performed using STRING (40).

Western blot analysis

Thirty μg of proteins were separated by 10% SDS-PAGE and then transferred to PVDF membranes (Millipore). After blocking for 2 h at room temperature with 5% (w/v) skimmed milk powder in TBS (100 mM Tris-HCl, 150 mM NaCl, pH 7.6), the membrane was incubated overnight at 4 °C with rabbit polyclonal antibodies against GNS, PLCB2, KRT26, or GADPH in antibody dilution buffer (5% (w/v) skimmed milk in TBST (0.05% (v/v) Tween 20 in TBS, pH 7.6)). The membranes were washed three times with TBST, and then incubated with alkaline phosphatase-conjugated secondary antibodies (1:1000 (v/v) in antibody dilution buffer) for 1 h at room temperature. The membranes were washed three times with TBST and proteins detected using a 5-bromo-4-chloro-3-indolyl phosphate/nitroblue tetrazolium salt substrate solution. β−Actin was used as the internal control.

Fluorescence immunohistochemistry

The anti-PLCB2 antibody was labeled with Cy3 fluorescence dye (GE Healthcare, Little Chalfont, UK) and purified by Sephadex G-25 columns according to the manufacturer's instructions. Adherent cells were fixed with 4% (w/v) paraformaldehyde and permeabilized at 4°C for 10 minutes in PBS supplemented with 1% (v/v) Triton X-100, then rinsed twice in PBS. The permeabilized cells were treated with H_2O_2 (3% (v/v) in methanol) for 20 min to block endogenous peroxidases. Cells were blocked with 5% (w/v) bovine serum albumin in PBS (blocking solution) for 1 h at room temperature. After that, cells were incubated with 100 μg/mL of Cy3 labeled PLCB2 antibody diluted in the blocking solution overnight at 4°C in the dark. Finally, cells were stained with DAPI (1 μg/mL in PBS; Roche) for 10 min before the final rinse. A laser scanning confocal microscope FV 1000 (Olympus, Tokyo, Japan) was used to collect the images using the merge channels of Cy3 and DAPI.

Results

Identification of N-glycoproteins

Relatively large indexes of the N-glycoproteomes from the activated LX-2 and the control were identified by LC-MS/MS. A total of 81 and 64 non-redundant N-glycopeptides representing 65 and 51 unique N-glycoproteins were identified in the activated and the quiescent LX-2 cells respectively (Table 1 and Figs. 2A and 2B). Of these N-glycoproteins, 35 proteins (e.g., pigment epithelium-derived factor and clathrin heavy chain 1) were identified specifically in the activated LX-2 cells, and 21 proteins (e.g., ZBTB1) were identified specifically in the control cells (Table 1). Estimates of emPAI-based protein abundance deviated from the

Table 1. N- glycoproteins / N-glycopeptides / N-glycosites identified from activated and quiescent LX-2 cells by hydrazide chemistry.

Accession	Glycoprotein	Gene	Protein Coverage %	Identified Glycopeptide[a]	Peptide Score	Q or A[b]	A/Q Ratio[c]	Glycosites[d]
IPI00003269	Beta-actin-like protein 2	ACTBL2	21.5	MTDNELSALVVDN*GSGMCKA	5.87	Q, A	—	13^{N}
IPI00010790	Biglycan	BGN	10.9	RMIEN*GSLSFLPTLRE	46.96	Q, A	—	270^{K}
IPI00045396	Calumenin	CALU	6.2	RN*VTYGTYLDDPDPDDGFNYKQ	85.32	Q, A	—	131^{K}
IPI00107357	Cleft lip and palate transmembrane protein 1	CLPTM1	2.2	KDYYPIN*ESLASLPLRV	84.02	Q, A	0.6	295^{K}
IPI00551062	Protein canopy homolog 3	CNPY3	7.9	KVVMDIPYELWN*ETSAEVADLKKQ	57.57	Q, A	2.7	153^{K}
IPI00297646	Collagen alpha-1(I) chain	COL1A1	1.0	RLMSTEASQN*ITYHCKN	52.31	Q, A	—	1365^{N}
IPI00739099	Collagen alpha-2(V) chain	COL5A2	6.5	KEASQN*ITYICKN	51.38	Q, A	—	1400^{P}
IPI00182126	Peptidyl-prolyl cis-trans isomerase FKBP9	FKBP9	6.7	RYHYN*GTFLDGTLFDSSHNRM RYHYN*GTLLDGTLFDSSYSRN	23.05 21.15	Q, A	—	174^{K}, 286^{K}
IPI00303300	Peptidyl-prolyl cis-trans isomerase FKBP10	FKBP10	5.3	RYHYN*GTFEDGKK RYHYN*GSLMDGTLFDSSYSRN	27.12 52.07	Q, A	0.57	70^{P}, 294^{P}
IPI00184854	cDNA: FLJ22221 fis, clone HRC01651	FKBP10	5.4	RYHYN*GSLMDGTLFDSSYSRN	44.37	Q, A	0.57	6^{N}
IPI00029723	MIR198 Follistatin-related protein 1	FSTL1	3.2	KGSN*YSEILDKY	54.04	Q, A	0.41	144^{P}
IPI00293088	Lysosomal alpha-glucosidase	GAA	2.4	RQVVEN*MTRAHFPLDVQWNDLDYMDSRR RGVFITN*ETGQPLIGKV	4.92 50.59	Q, A	0.58	390^{K}, 470^{K}
IPI00012102	N-acetylglucosamine-6-sulfatase	GNS	15.9	KYYN*YTLSINGKA RQAKTPMTN*SSIQFLDNAFRK KMLVANIDLGPTILDIAGYDLN*KT	55.24 2.61 7.17	Q, A	2.03	183^{K}, 279^{K}, 387^{K}
IPI00027851	cDNA FLJ53927, highly similar to Beta-hexosaminidase alpha chain	HEXA	1.9	KSAEGTFFIN*KT	43.34	Q, A	2.03	157^{K}
IPI00760554	HLA class I histocompatibility antigen, A-69 alpha chain	HLA-A	4.1	RGYYN*QSEAGSHTVQRM	35.06	Q, A	0.6	110^{N}
IPI00022488	Hemopexin	HPX	2.8	RSWPAVGN*CSSALRW	51.61	Q, A	—	187^{K}
IPI00003865	Heat shock cognate 71 kDa protein	HSPA8	38.2	KN*QTAEKEEFEHQQKE	18.01	Q, A	—	584^{N}
IPI00555565	Putative heat shock protein HSP 90-beta 4	HSP90AB4P	10.5	MSLIINTFYSNKEIFLQELISN*ASDALDKI	10.62	Q, A	0.45	22^{N}
IPI00027230	Endoplasmin	HSP90B1	14.7	RELISN*ASDALDKI KHNN*DTQHIWESDSNEFSVIADPRG KYN*DTFWKEFGTNIKL	11.39 32.93 1.56	Q, A	—	107^{K}, 217^{K}, 481^{P}
IPI00000877	Hypoxia up-regulated protein 1	HYOU1	3.6	RVFGSQN*LTTVKL	18.45	Q, A	—	515^{K}
IPI00020557	Prolow-density lipoprotein receptor-related protein 1	LRP1	1.3	RFN*STEYQVVTRV RIETILLN*GTDRK RMHLN*GSNVQVLHRT	33.44 47.6 11.53	Q, A	—	446^{K}, 729^{K}, 3089^{K}

IPI00337335	Myosin-14	MYH14	4.4	RAQAELEN*VSGALNEAESKTIRL	15.91	Q, A	—	1308^{N}
IPI00335168	Myosin light polypeptide 6	MYL6	45.7	RVFDKEGN*GTVMGAEIRH	65.97	Q, A	—	101^{N}
IPI00025049	Cation-dependent mannose-6-phosphate receptor	M6PR	14.8	RLN*ETHIFN*GSNWIMLIYKG	67.32	Q, A	—	107^{K}, 113^{P}
IPI00337495	Procollagen-lysine,2-oxoglutarate 5-dioxygenase 2	PLOD2	4.9	KYFN*YTVKV	15.53	Q, A	—	63^{P}, 696^{P}
				RYN*CSIESPRK	53.55			
IPI00479743	POTE ankyrin domain family member E	POTEE	12.1	KHESNNVGLLEN*LTNGVTAGNGDNGLIPQRK	2.62	Q, A	—	432^{N}, 648^{N}, 712^{N}
				KEKDVLHEN*STLRE	2.98			
				KALQLNELTMDDDTAVLVIDN*GSGMCKA	5.38			
IPI00009923	Prolyl 4-hydroxylase subunit alpha-1	P4HA1	8.1	KDMSDGFISN*LTIQRQ	3.18	Q, A	—	113^{K}
IPI00015842	Reticulocalbin-1	RCN1	8.8	RVVRPDSELGERPPEDN*QSFQYDHEAFLGKE	39.12	Q, A	—	53^{K}
IPI00887938	Protein SET	SET	4.4	KEFHLN*ESGNPSSKS	41.17	Q, A	—	159^{N}
IPI00030847	Transmembrane 9 superfamily member 3	TM9SF3	1.9	RIVDVN*LTSEGKV	32.24	Q, A	1.81	174^{K}
IPI00219678	Eukaryotic translation initiation factor 2 subunit 1	EIF2S1	13.0	RAGLN*CSTENMPIKI	1.73	Q	0.01	217^{N}
IPI00642244	ER membrane protein complex subunit 1	EMC1	1.0	RFINYN*QTVSRM	17.23	Q	0.01	913^{K}
IPI00339269	Heat shock 70 kDa protein 6	HSPA6	5.0	RELAVGIDLGTTYSCVGVFQQGRVEILANDQGN*RT	1.01	Q	0.01	37^{N}
IPI00442154	leucine-, glutamate- and lysine-rich protein 1	LEKR1	6.6	KEIDSN*DSVSENLRKE	25.66	Q	0.01	214^{N}
IPI00470649	Nicalin	NCLN	1.4	RVIYN*LTEKG	15.08	Q	0.01	428^{P}
IPI00218830	Glycylpeptide N-tetradecanoyltransferase 1	NMT1	8.4	KMKGFDVFNALDLMEN*KT	2.12	Q	0.01	458^{N}
IPI00873495	DNA polymerase theta	POLQ	4.4	KINEVLIQN*GSKNQNVYMKH	1.72	Q	0.01	1309^{N}
IPI00419585	Peptidyl-prolyl cis-trans isomerase A	PPIA	38.2	KHTGPGILSMANAGPNTN*GSQFFICTAKT	126.71	Q	0.01	108^{K}
IPI00657716	Peptidylprolyl cis-trans isomerase A-like 4G	PPIAL4B	20.7	KHTGSGILSMANAGPNTN*GSQFFICTAKT	2.81	Q	0.01	108^{N}
IPI00425902	Translocon-associated protein subunit beta	SSR2	8.4	RIAPASN*VSHTVVLRPLKA	56.73	Q	0.01	88^{K}
IPI00025160	Protein VAC14 homolog	VAC14	6.9	KEVANVCN*QSLMKL	0.82	Q	0.01	325^{N}
IPI00479509	RcNSEP1 (Fragment)	YBX1	46.7	KGAKAAN*VTGPGGVPVQGSKY	77.4	Q	0.01	120^{N}
IPI00007273	Zinc finger and BTB domain-containing protein 1	ZBTB1	6.5	RMFFMNHQHSTAQLN*LSNMKI	3.06	Q	0.01	64^{N}
IPI00936175	LOC100128355 similar to hCG1790904	LOC100128355	10.8	KFMENANYGIEGMQVNN*VSKAVN*KS	0.23	Q	0.01	N
IPI00935692	LOC100290509 hypothetical protein XP_002348229	LOC100290509	32.4	KHTGPGILSMANAGPNMN*GSQFFICTAKT	1.63	Q	0.01	N
IPI00886911	LOC646048 similar to actin alpha 1 skeletal muscle protein	LOC646048	10.6	RAQSLALATLPPIHARCQLTMDDDIEVLVVNN*GSGMCKV	3.12	Q	0.01	N
IPI00877807	21 kDa protein		45.9	RNVLIFDLGDDTFN*VSILTTEDGIFEVKS	2.42	Q	0.01	N
IPI00879182	8 kDa protein		45.9	KHTGPGMLSMANAGPNTN*GSQFLICTAKT	12.46	Q	0.01	N

IPI00908994	cDNA FLJ51587, highly similar to Heterogeneous nuclear ribonucleoprotein A1		23.6	KKIFVGGSYNDFGNYNN*QSSNFGPMKG	3.44	Q	0.01	121^{N}
IPI00922838	cDNA FLJ56074, highly similar to 150 kDa oxygen-regulated protein		8	RVFGSQN*LTTVKL KN*ATLAEQAKL	18.45 0.06	Q	0.01	559^{N}, 851^{N}
IPI00453476	cDNA FLJ51983, highly similar to Phosphoglycerate mutase 1		55.5	RSYDVPPPPMEPDHPFYSN*ISKD	15.52	Q	0.01	120^{N}
IPI00021439	Actin, cytoplasmic 1	ACTB	61.1	MDDDIAALVVDN*GSGMCKAGFAGDDAPRA	1.73	A	100	12^{N}
IPI00021812	Neuroblast differentiation-associated protein AHNAK	AHNAK	3.1	KAPN*ISMPDVDLNLKGPKI	7.5	A	100	2452^{N}
IPI00760877	Transcription factor TFIIIB component B	BDP1	3.2	KATGN*ESSPRE	18.96	A	100	962^{N}
IPI00024067	Clathrin heavy chain 1	CLTC	4.9	KEAIDSYIKADDPSSYMEVVQAAN*TSGNWEELVKY	8.13	A	100	1145^{N}
IPI00215637	ATP-dependent RNA helicase DDX3X	DDX3X	13	MSHVAVENALGLDQQFAGLDLN*SSDN*QSGGSTASKG	3.71	A	100	22^{N}, 26^{N}
IPI00302453	Dynein heavy chain 9, axonemal	DNAH9	2.6	KQSISKFMAFVHTSVN*QTSQSYLSNEQRY RMSVEN*ATILINCERWPLMVDPQLQGIKW	1.37 4.4	A	100	3023^{N}, 3452^{N}
IPI00414676	Heat shock protein HSP 90-beta	HSP90AB1	28.3	RELISN*ASDALDKI	11.39	A	100	46^{N}
IPI00930442	Putative uncharacterized protein DKFZp686M24218	IGHG4	1.9	REEQFN*STYRV	29.99	A	100	177^{K}
IPI00306604	Integrin alpha-5	ITGA5	1.8	RHPGN*FSSLSCDYFAVN*QSRL	27.31	A	100	712^{P}, 724^{P}
IPI00220327	Keratin, type II cytoskeletal 1	KRT1	18.6	RMSGECAPN*VSVSVSTSHTTISGGGSRG	1.56	A	100	500^{N}
IPI00009865	Keratin, type I cytoskeletal 10	KRT10	25	RN*VSTGDVNVEMNAAPGVDLTQLLNNMRS	9.34	A	100	296^{N}
IPI00015309	Keratin, type I cytoskeletal 12	KRT12	4.3	MDLSN*NTMSLSVRT	7.87	A	100	5^{N}
IPI00375910	Keratin, type I cytoskeletal 26	KRT26	12	RQIISATICN*ASIVLQNDNARLTADDFRL	0.39	A	100	155^{N}
IPI00376379	keratin, type II cytoskeletal 1b	KRT77	7.3	KMEIAELN*RTVQRL	7.47	A	100	386^{N}
IPI00216070	Myosin light chain 1/3, skeletal muscle isoform	MYL1	14.4	RVFDKEGN*GTVMGAELRH	65.97	A	100	144^{N}
IPI00793089	Myosin light polypeptide 6	MYL6B	53	RVFDKEGN*GTVMGAEIRH	3.69	A	100	101^{N}
IPI00220278	Myosin regulatory light polypeptide 9	MYL9	44.2	KNPTDEYLEGMMSEAPGPIN*FTMFLTMFGEKL	6.6	A	100	82^{N}
IPI00169285	Putative phospholipase B-like 2	PLBD2	8	RSDLNPAN*GSYPFQALRQ	34.77	A	100	515^{K}
IPI00784327	1-phosphatidylinositol 4,5-bisphosphate phosphodiesterase beta-2	PLCB2	5.1	REIN*NSHIQEVVQVIKQ	6.27	A	100	1076^{N}
IPI00739539	POTE ankyrin domain family member F	POTEF	11.7	KHESNNVGLLEN*LTNGVTAGNGDNGLIPQRK	1.29	A	100	432^{N}, 712^{N}
IPI00738655	POTE ankyrin domain family member J	POTEJ	14.2	KALQLNELTMDDDTAVLVIDN*GSGMCKA	5.38	A	100	675^{N}
IPI00887316	Actin, beta-like 3	POTEKP	12.1	KALQLNELTMDDDTAVLVIDN*GSGMCKA KHGSTHVGFPEN*LTNGAAAGNGDDGLIPPRKS	5.38 1.33	A	100	N
IPI00925411	13 kDa protein	PPIA	48.3	KHTGPGILSMANAGPNTN*GSQFFICTAKT	131.94	A	100	48^{N}

IPI00550991	cDNA FLJ35730 fis, highly similar to ALPHA-1-ANTICHYMOTRYPSIN	SERPINA3	10.5	RTLN*QSSDELQLSMGNAMFVKE	4.12	A	100	127^{K}
IPI00006114	Pigment epithelium-derived factor	SERPINF1	5.3	KVTQN*LTLIEESLTSEFIHDIDRE	94.11	A	100	285^{K}
IPI00844215	Spectrin alpha chain, brain	SPTAN1	2.8	RQEQIDN*QTRI	1.59	A	100	1051^{N}
IPI00604442	Translocon-associated protein subunit beta	SSR2	30.8	RIAPASN*VSHTVVLRPLKA	35.07	A	100	88^{K}, 114K
				KAGYFN*FTSATITYLAQEDGPVVVSCPNP	1.49			
IPI00218905	TRAF2 and NCK-interacting protein kinase	TNIK	3.9	KGLSGFQEALN*VTSHRVEMPRQ	0.5	A	100	627^{N}
IPI00877930	Tubulin beta-8 chain	TUBB8	24.4	KN*SSYFADWLPDNVKT	2.66	A	100	337^{N}
IPI00291175	Vinculin	VCL	13.7	KATMLGRTN*ISDEESEQATEMLVHNAQNLMQSVKE	2.37	A	100	1078^{N}
IPI00022774	Transitional endoplasmic reticulum ATPase	VCP	21.3	RAVAN*ETGAFFFLINGPEIMSKLAGESESNLRK	0.81	A	100	260^{N}
IPI00640611	LOC100288889 hypothetical protein XP_002342830	LOC100288889	49.4	KAQFN*LSVYPYDPTWSITHTEETLVLVMANKN	1.96	A	100	N
IPI00910712	cDNA FLJ57036, highly similar to Homo sapiens tropomyosin 2 (beta) (TPM2)		20.1	RTMDQALKSLMASEEEVVTPMN*LSGQWRL	1.38	A	100	219^{N}
IPI00921849	cDNA FLJ57046, highly similar to Lysosomal alpha-glucosidase		11	RGVFITN*ETGQPLIGKV	50.59	A	100	470^{N}
IPI00964079	cDNA FLJ58784, highly similar to T-complex protein 1 subunit epsilon		15.2	MN*SSLGPTIEKLSVSHIMAAKA	5.53	A	100	2^{N}

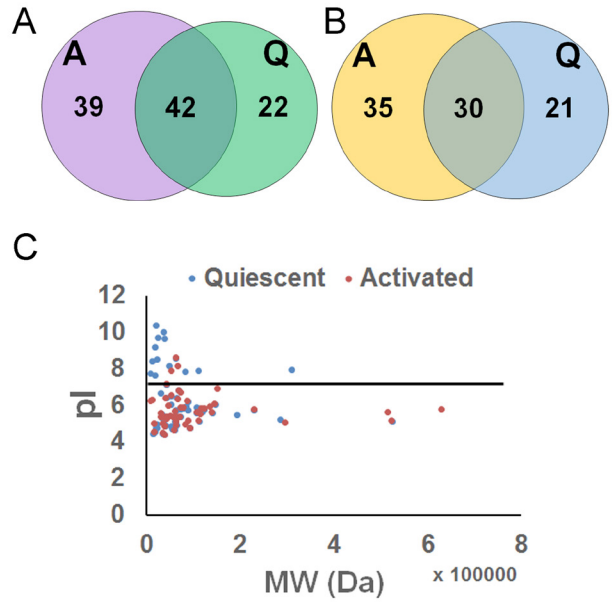

Figure 2. Identification and physiochemical characteristics of N-glycoproteins isolated from activated and quiescent LX-2 cells. The Venn diagrams present the numbers of non-redundant N-glycopeptides (A) and N-glycoproteins (B) identified by MS. A: activated LX-2 cells. Q: quiescent LX-2 cells. (C) A pI-molecular weight diagram of total N-glycoproteins in LX-2 cells.

actual measured values and revealed that four proteins (e.g., N-acetylglucosamine-6-sulfatase and transmembrane 9 superfamily member 3) were up-regulated (fold-change > 1.5), while 7 proteins (e.g., lysosomal α-glucosidase and putative heat shock protein HSP 90-β 4) were down-regulated (fold-change < 0.67) in the activated LX-2 cells compared to the control. By mapping to the Uniprot database (41), 23 proteins (26.7% of those identified in this research) were marked as N-glycoproteins, 5 were potential N-glycoproteins (5.8%), and 58 were newly identified N-glycoproteins (67.4%). After identification of the isoelectric point (pI) and molecular weights, the pI values of the total identified N-glycoproteins were between 4 and 11, but most of these were clustered around 4-6 in the activated compared to the quiescent LX-2 cells. The molecular weight of most N-glycoproteins (90.7%) was lower than 200 kDa (Fig. 2C).

N-Glycosites identified in LX-2 cells by hydrazide chemistry

Totally, 103 non-redundant N-glycopeptides with 107 glycosites from 86 N-glycoproteins were identified in this study by LC-MS/MS. By mapping all 107 glycosites to the Uniprot database, 33 (30.8%) of the identified N-glycosites were annotated as "known" (e.g., N^{515}LT on hypoxia up-regulated protein 1), and 11 (10.3%) are marked as "potential" sites of N-glycosylation (e.g., N^{481}DT on endoplasmin). The other 63 glycosites (58.9%) were new ones (e.g., N^{1308}VS on myosin-14) identified in this study (Table 1). Besides, 41 and 23 N-glycosites were presented solely in the activated and the quiescent LX-2 cells respectively (Table 1).

Gene ontology analysis

To identify the major biological functions of N-glycoproteins in LX-2 cells, Blast2go was used to analyze three aspects of the N-glycoproteins that were identified: cellular components, biological processes, and molecular functions (Fig. 3A). Totally, 77 of 86 identified N-glycoproteins had GO annotations. In terms of the cellular components, 63 (73.3%) were cell proteins while 54 (62.8%) were organelle proteins. Other proteins were located on membranes (27, 31.4%), macromolecular complexes (25, 29.1%), and membrane-enclosed lumens (16, 18.6%). In terms of biological processes, 50 (58.1%), 39 (45.3%), 37 (43.0%), and 34 (39.5%) proteins participated in cellular processes, responses to stimuli, metabolic processes, and biological regulation, respectively. In terms of molecular functions, glycoproteins with binding properties contributed the most (57, 66.3%), but other molecular functions including catalytic (22, 25.6%), structural molecule (17, 19.8%), and receptor (4, 4.7%) activities were also found. Detailed analysis of the glycoprotein binding properties revealed that large proportions of the binding activity were to proteins (31, 36.0%), small molecules (22, 25.6%), ion (20, 23.3%), and carbohydrates (6, 7.0%).

A GO enrichment analysis was performed to determine whether there was any difference in the three aspects of GO annotations between the activated and quiescent LX-2 cells. The response to a stimulus, detection of a stimulus, activation of an immune response, and gene silencing were much higher, while the initiation of translation and cell cycle progression were much lower, in the activated than in the quiescent LX-2 cells (Fig. 3B).

KEGG pathway and protein interaction network analysis

Sixty seven of the total 86 identified N-glycoproteins were annotated in DAVID Bioinformatics Resources 6.7 with the thresholds of counts > 2 and P values < 0.05 compared to the background of the human genome. These N-linked glycoproteins mapped to 11 KEGG pathways (e.g., regulation of actin cytoskeleton, focal adhesion, and tight junction) that were significantly represented ($p < 0.05$) with a fold enrichment higher than 4.5 (Table S1). Proteins involved in focal adhesion (e.g., collagen alpha-2(V) chain, integrin alpha-5, vinculin, and cytoplasmic 1) (Fig. 4A) and glycosaminoglycan degradation (e.g., N-acetylglucosamine-6-sulfatase and the beta-hexosaminidase alpha chain) (Fig. 4B) were identified or up-regulated in the activated LX-2 cells. Upon further annotation, 83.6% of these N-glycoproteins had a signal peptide and contained N-linked glycosylation sites (Table S2). In addition, a total of 73 matched N-glycoproteins were queried against the STRING Homo sapiens database to determine their functional relevance (Fig. 5A). Through K-mean clustering analysis, the clusters of CCT5, VCP, HSP90AB1, and ACTB; SERPINA3, CNPY3, and SERPINF1; POTEJ, POTEF, POTEI, and TUBB8; and MYL1, MYL9, MYL6B, CLTC, and SPTAN1, were all up-regulated in activated LX-2 cells.

Validation of N-glycoproteins expression in LX-2 cells

Alterations of N-glycoproteins expression in activated compared to quiescent LX-2 cells were assessed

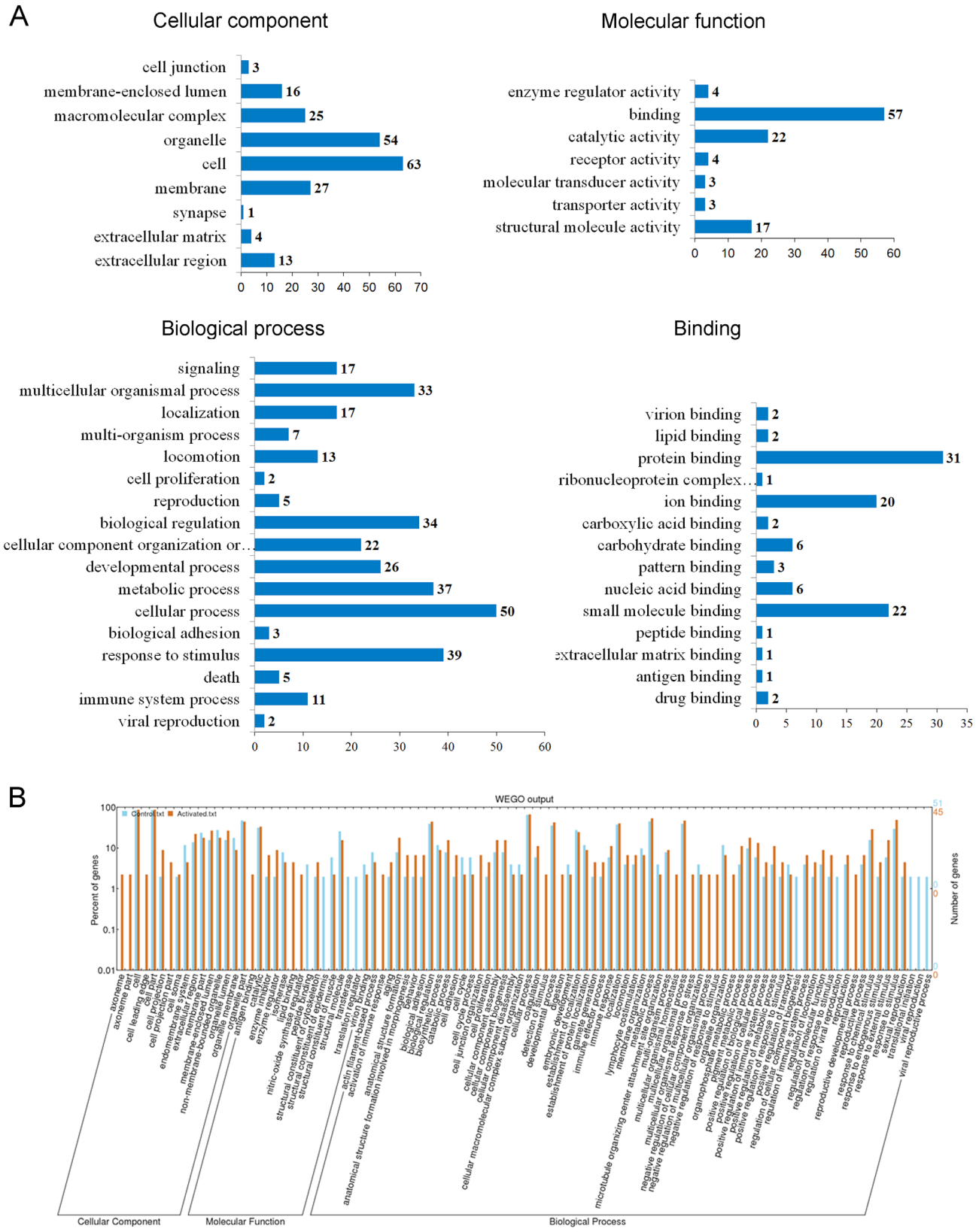

Figure 3. Gene ontology annotations of the N-glycoproteins identified in LX-2 cells. (A) Total N-glycoproteins identified in LX-2 cells were analyzed using Blast2GO® software for functional enrichment according to three grouping classifications: cellular components, biological processes, and molecular functions. (B) Gene ontology classification, and comparison of the enrichment of functional groups between quiescent and activated LX-2 cells, were performed using WEGO software.

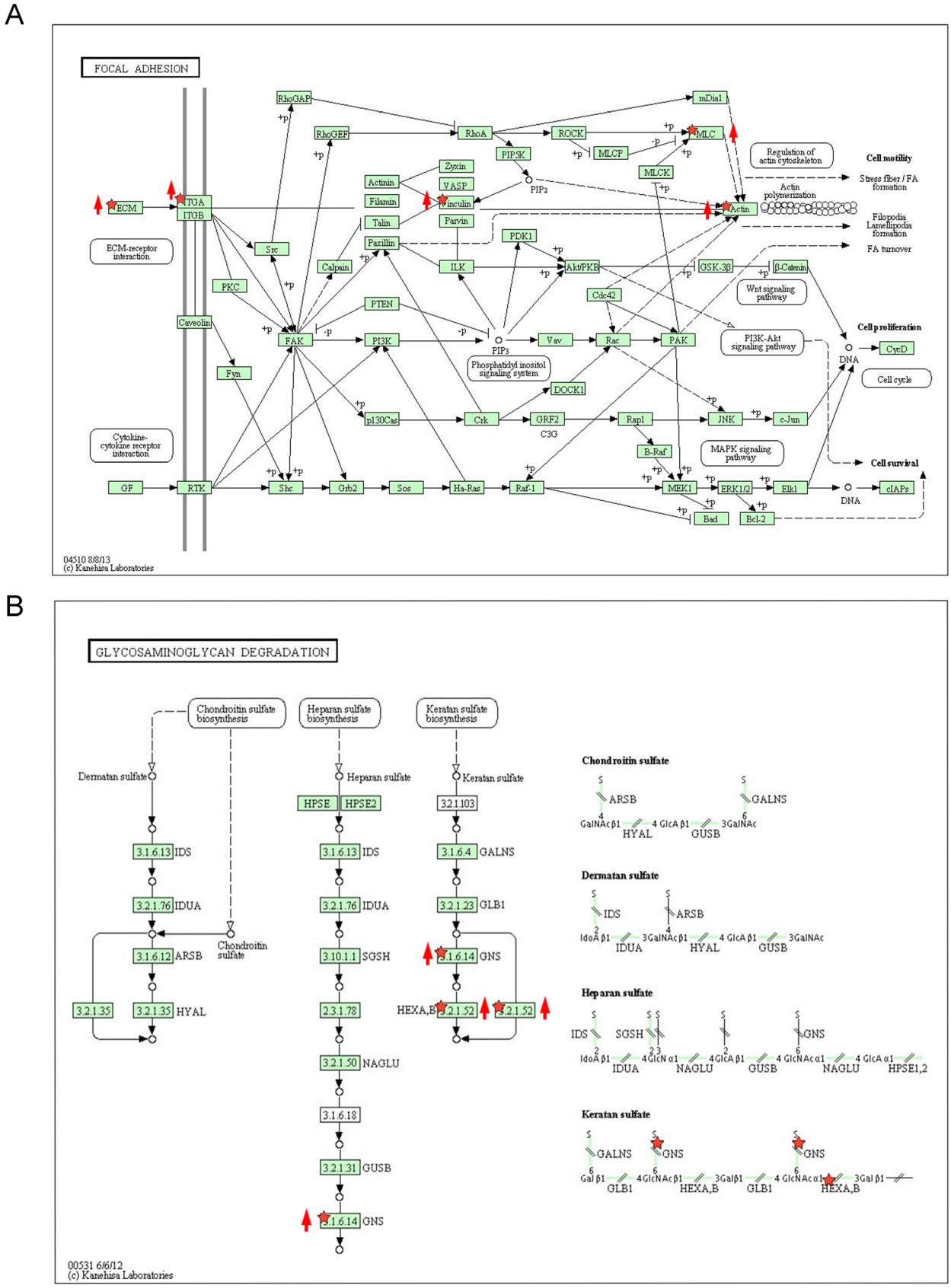

Figure 4. KEGG pathway analysis of N-glycoproteins identified in activated LX-2 cells. (A) N-Glycoproteins (red star) involved in focal adhesion, and (B) glycosaminoglycan degradation, were identified or up-regulated (red arrow) in activated LX-2 cells.

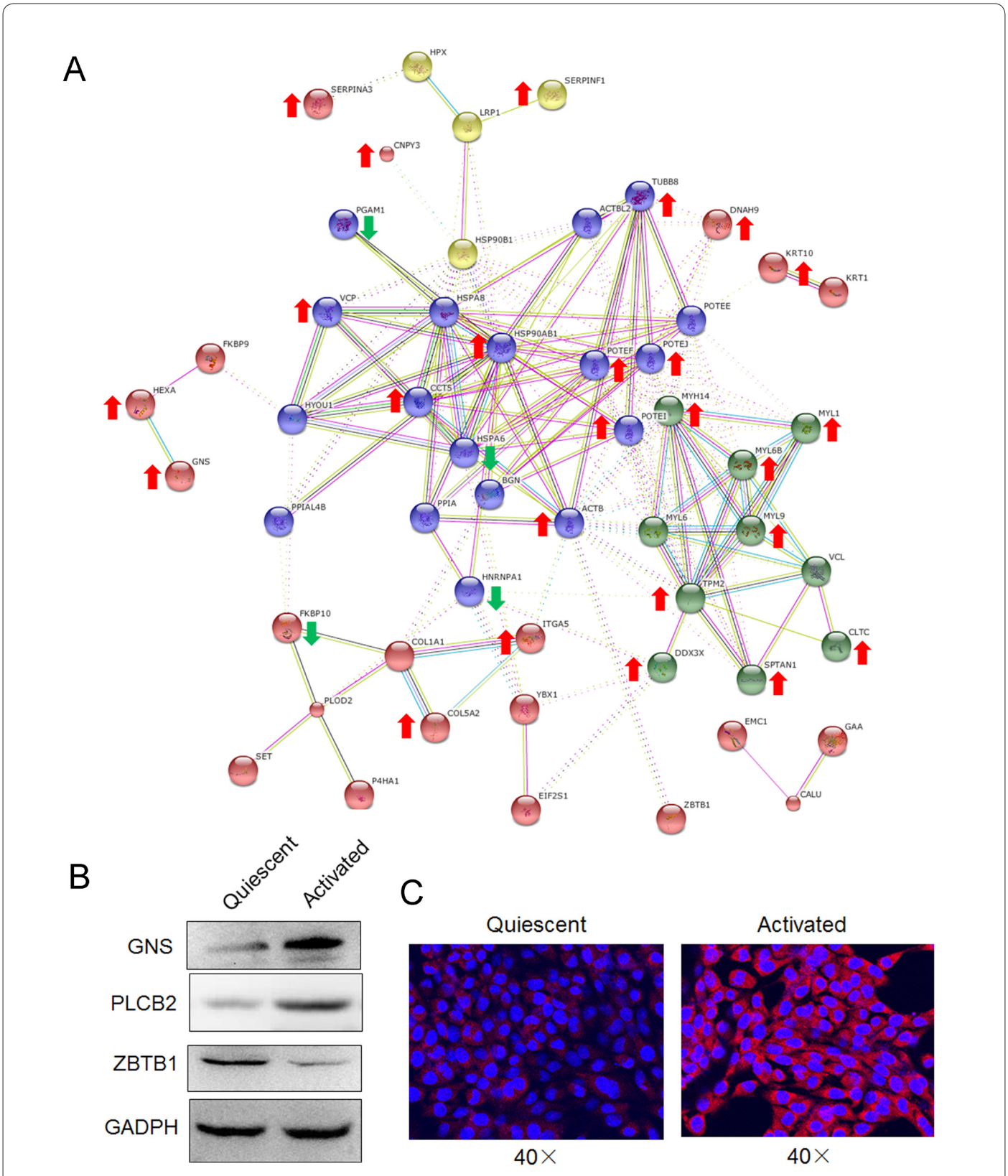

Figure 5. Functional protein association networks of N-glycoproteins and validation of the expression of N-glycoproteins in LX-2 cells. (A) Potential interactions among N-glycoproteins showing significant correlations by STRING analysis. Up-regulated (red arrow) and down-regulated (green arrow) proteins in activated LX-2 cells. (B) Western blots of GNS, PLCB1, and ZBTB1 in activated and control LX-2 cells. (C) Expression and location of PLCB2 in quiescent and activated LX-2 cells using fluorescence immunohistochemistry. The images were obtained using a 40× objective lens.

by measuring the expression of N-acetylglucosamine-6-sulfatase (GNS), 1-phosphatidylinositol 4,5-bisphosphate phosphodiesterase beta-2 (PLCB2), and zinc finger and BTB domain-containing protein 1 (ZBTB1). The expression of GNS and PLCB2 were increased and the expression of ZBTB1 was decreased in the activated versus the quiescent LX-2 cells, which was consistent with the result of MS identification (Fig. 5B). Immunohistochemistry showed obviously the increased expression of PLCB2 in activated LX-2 cells than the control (Fig. 5C).

Discussion

Protein N-glycosylation is importantly involved in almost all pivotal cellular processes, such as ion transport, bacterial and viral infection, cell communication, and signal transduction (42-44). Aberrant N-glycosylation is related to abnormal development, inflammation, carcinogenesis, and tumor progression (45,46). Most of current tumor biomarkers are N-glycoproteins (e.g., prostate-specific antigen, α-fetoprotein, and HER2/neu) (47). Comparison of profiles of N-glycoproteins in human HSCs with and without activation by TGF-β1 by LC-MS/MS was particularly useful method for finding novel molecular mechanisms of HSC activation and antifibrotic therapeutic strategies. However, high-efficiency enrichment of N-glycoproteins or N-glycopeptides before MS detection is usually the first step of N-glycoproteome analysis due to the relative lower abundance of N-glycoproteins in complex biological samples. The N-glycopeptide extraction method based on hydrazide chemistry is very easy to handle, exhibits high specificity and high reproducibility, and is widely used in serum glycoproteome research, glycosylation analyses of the influenza virus, and disease-related glyco-biomarker discovery (48,49). In this study, more N-glycoproteins and N-glycosites were identified from activated than from quiescent LX-2 cells. In our previous study, PHA-E, that recognizes bisecting GlcNAc and biantennary N-glycans, showed increased binding to the cytoplasmic membrane and the perinuclear region of cytoplasm in activated LX-2 cells. In contrast, PHA-E+L, that binds specifically to tri- and tetra-antennary complex-type N-glycans, showed no significant difference between the two cell groups. This suggests that the higher abundance of N-glycoproteins and N-glycosites in activated HSCs might be the result of increased amounts of bisecting GlcNAc and biantennary N-glycans.

The activation of the HSCs is characterized by proliferation, contractility, fibrogenesis, and chemotaxis, especially the accumulation of ECM (52). In this study, most proteins involved in regulation of the actin cytoskeleton (e.g., vinculin, myosin light chains, and integrin alpha-5) and focal adhesion (e.g., collagen alpha-2(V) chain, integrin alpha-5, vinculin, and cytoplasmic 1) (Fig. 4A) were identified solely or up-regulated in the activated HSCs. Actin cytoskeleton participates in many basical processes including the regulation of cell shape, motility, and adhesion (50). Focal adhesions are specific large macromolecular assemblies through which the cytoskeleton of a cell connects to the ECM. Proteins associate and disassociate with the ECM continually as signals are transmitted to other parts of the cell, relating to anything from cell motility to the cell cycle (51). Each of these characteristics is closely related to regulation of the actin cytoskeleton and focal adhesion. Furthermore, according to the protein interaction networks, many cytoskeletal proteins and proteins attached to the cytoskeleton are up-regulated in the activated HSCs. Actually, the changes in the abundance of N-glycopeptides from the LC/MS experiments may be caused by either changes in protein expression or changes in N-glycosylation, or both of them. To elucidate aberrant glycosylation on the function of those proteins, more research needs to be done in future.

The cytoskeleton of eukaryotes has three major components: microfilaments, microtubules, and intermediate filaments. In the current study, ankyrin domain family members (i.e., POTEJ, POTEF, POTEKP), microtubule proteins (i.e., TUBB8), myosin light chains (i.e., MYL1, MYL9, MYL6B) that attach to the microfilament and "walk" along them, clathrin (i.e., CLTC), spectrin (i.e., SPTAN1) that exists as a fibrous coating on the inner cytoplasmic surface of membranes, and keratins (i.e., KRT10, KRT12, KRT16, and KRT77) belonging to intermediate filament proteins, were expressed at distinctly higher levels in the activated LX-2 cells (Fig. 5A and Table 1). In early stages of fibrosis, activated stellate cells already show features of smooth muscle–like cells, characterized by expression of a number of contractile filaments, including smooth muscle actin (53) and myosin (54), that generate calcium-dependent and -independent contractile forces contributing to cellular contractility (55,56). Overall, the regulation of cytoskeleton-related pathways involving N-glycoproteins, and the increased expression of cytoskeletal N-glycoproteins seen in this study, were largely responsible for the contractility of HSCs activated by TGF-β1.

GNS, with multiple known N-glycosites, that was up-regulated in activated HSCs (Table 1 and Fig. 5B), is a lysosomal enzyme responsible for hydrolysis of the N-acetyl-D-glucosamine 6-sulfate units of heparan sulfate and keratan sulfate. Heparan sulfate proteoglycans are found at the cell surface and in the ECM, where they interact with a plethora of ligands (57). Increased GNS activity increases the degradation of heparan sulfate, affecting crucial cell signaling pathways, such as those involving Wnt, Hedgehog, TGF-β1, and fibroblast growth factor (58). The N-glycoprotein PLCB2 was found only in activated HSCs. Western blot and immunohistochemistry analyses also showed an increased expression level of PLCB2 in activated HSCs compared to control cells. This enzyme catalyzes the formation of inositol 1,4,5-trisphosphate and diacylglycerol from phosphatidylinositol 4,5-bisphosphate using calcium as a cofactor. PLCB2 plays an important role in the intracellular transduction of many extracellular signals including the calcium signaling pathway, chemokine signaling pathway, phosphatidylinositol signaling system, carbohydrate digestion and absorption, and the Wnt signaling pathway (59).

In conclusion, increased expression of N-glycoproteins and N-glycosites play important roles in cellular contractility, signal transduction, and responses to stimuli, and might provide useful information for discovering novel molecular mechanism of HSC activation and new therapeutic targets in liver fibrosis.

Acknowledgements

This work was supported by National Natural Science Foundation of China (No. 81401137), the Fundamental Research Funds for the Central Universities, China (No. XJJ2014069), and China Postdoctoral Science Foundation (No. 2015M572574).

References

1. Sánchez-Valle, V., Chávez-Tapia, N.C., Uribe, M. and Mén-

dez-Sánchez, N. Role of oxidative stress and molecular changes in liver fibrosis: a review. *Curr. Med. Chem.* 2012, **19**: 4850-4860. doi: 10.2174/092986712803341520.

2. Muhanna, N., Doron, S., Wald, O., Horani, A., Eid, A. and Pappo, O. Activation of hepatic stellate cells after phagocytosis of lymphocytes: A novel pathway of fibrogenesis, *Hepatology* 2008, **48**: 963-977. doi: 10.1002/hep.22413.

3. Troeger, J.S., Mederacke, I., Gwak, G.Y., Dapito, D.H., Mu, X. and Hsu, C.C. Deactivation of hepatic stellate cells during liver fibrosis resolution in mice. *Gastroenterology* 2012, **143**: 1073–1083. doi: 10.1053/j.gastro.2012.06.036.

4. Liu, C., Li, J., Xiang, X., Guo, L., Tu, K. and Liu, Q. PDGF receptor-α promotes TGF-β signaling in hepatic stellate cells via transcriptional and posttranscriptional regulation of TGF-β receptors. *Am. J. Physiol. Gastrointest. Liver Physiol.* 2014, **307**: G749-G759. doi: 10.1152/ajpgi.00138.2014.

5. Shimada, H., Staten, N.R. and Rajagopalan, L.E. TGF-β1 mediated activation of Rho kinase induces TGF-β2 and endothelin-1 expression in human hepatic stellate cells. *J. Hepatol.* 2011, **54**: 521-528. doi: 10.1016/j.jhep.2010.07.026.

6. Hart, G.W. and Copeland, R.J. Glycomics hits the big time. *Cell* 2010, **143**: 672-676. doi: 10.1016/j.cell.2010.11.008.

7. Breitling, J. and Aebi, M. N-linked protein glycosylation in the endoplasmic reticulum. *Cold Spring Harb Perspect Biol.* 2013, **5**: a013359. doi: 10.1101/cshperspect.a013359.

8. Kim, J.I. and Park, M.S. N-linked glycosylation in the hemagglutinin of influenza A viruses. *Yonsei Med. J.* 2012, **53**: 886-893. doi: 10.3349/ymj.2012.53.5.886.

9. Scott, H. and Panin, V.M. The role of protein N-glycosylation in neural transmission. *Glycobiology* 2014, **24**: 407-417. doi: 10.1093/glycob/cwu015.

10. Tian, Y. and Zhang, H. Characterization of disease-associated N-linked glycoproteins. *Proteomics* 2013, **13**: 504-511. doi: 10.1002/pmic.201200333.

11. Varelas, X., Bouchie, M.P. and Kukuruzinska, M.A. Protein N-glycosylation in oral cancer: dysregulated cellular networks among DPAGT1, E-cadherin adhesion and canonical Wnt signaling. *Glycobiology* 2014, **24**: 579-591. doi: 10.1093/glycob/cwu031.

12. Liu, T., Qian, W.J., Gritsenko, M.A., Camp, D.G., Monroe, M.E. and Moore, R.J. Human plasma N-glycoproteome analysis by immunoaffinity subtraction, hydrazide chemistry, and mass spectrometry. *J. Proteome Res.* 2005, **4**: 2070-2080. doi: 10.1021/pr0502065.

13. Yaping, Z., Ying, W., Luqin, D., Ning, T., Xuemei, A. and Xixian, Y. Mechanism of interleukin-1β-induced proliferation in rat hepatic stellate cells from different levels of signal transduction. *APMIS* 2014, **122**: 392-398. doi: 10.1111/apm.12155.

14. Muchmore, A.V. and Decker, J.M. The lectin-like interaction between recombinant tumor necrosis factor and uromodulin. *J. Immunol.* 1987, **138**: 2541–2546.

15. Cebo, C., Dambrouck, E., Maes, C., Laden, G., Strecker, J.C. and Michalski, J.P. Recombinant human interleukins IL-1alpha, IL-1beta, IL-4, IL-6, and IL-7 show different and specific calcium-independent carbohydrate-binding properties. *J. Biol. Chem.* 2001, **276**: 5685–5691. doi: 10.1074/jbc.M008662200.

16. Spratte, J., Meyer Zu Schwabedissen, H., Endlich, N., Zygmunt, M., and Fluhr, H. Heparin inhibits TNF-α signaling in human endometrial stromal cells by interaction with NF-κB. *Mol. Hum. Reprod.* 2013, **19**: 227-236. doi: 10.1093/molehr/gas060.

17. Qin, Y., Zhong, Y., Dang, L., Zhu, M., Yu, H., Chen, W. and Cui, J. Alteration of protein glycosylation in human hepatic stellate cells activated with transforming growth factor-β1. *J. Proteomics* 2012, **75**: 4114–4123. doi: 10.1016/j.jprot.2012.05.040.

18. Zhang, H., Li, X.J., Martin, D.B. and Aebersold, R. Identification and quantification of N-linked glycoproteins using hydrazide chemistry, stable isotope labeling and mass spectrometry. *Nature Biotech.* 2003, **21**: 660-666. doi: 10.1038/nbt827.

19. Tian, Y.A., Zhou, Y., Elliott, S., Aebersold, R. and Zhang, H. Solid-phase extraction of N-linked glycopeptides. *Nat. Protoc.* 2007, **2**: 334-339. doi:10.1038/nprot.2007.42.

20. Kaji, H., Saito, H., Yamauchi, Y., Shinkawa, T., Taoka, M. and Hirabayashi, J. Lectin affinity capture, isotope-coded tagging and mass spectrometry to identify N-linked glycoproteins. *Nat. Biotech*. 2003, **21**: 667-672. doi: 10.1038/nbt829.

21. Kaji, H., Yamauchi, Y., Takahashi, N. and Isobe. T. Mass spectrometric identification of N-linked glycopeptides using lectin-mediated affinity capture and glycosylation site-specific stable isotope tagging. Nat. Protoc. 2007, **1**: 3019-3027. dol: 10.1038/nprot.2006.444.

22. Sturiale, L., Barone, R., Palmigiano, A., Ndosimao, C.N., Briones, P. and Adamowicz, M. Multiplexed glycoproteomic analysis of glycosylation disorders by sequential yolk immunoglobulins immunoseparation and MALDI-TOF MS. *Proteomics* 2008, 8: 3822-3832. doi: 10.1002/pmic.200700496.

23. Cho, W., Jung, K. and Regnier, F.E. Use of glycan targeting antibodies to identify cancer-associated glycoproteins in plasma of breast cancer patients. *Anal. Chem.* 2008, 80: 5286-5292. doi: 10.1021/ac8008675.

24. Sparbier, K., Asperger, A., Resemann, A., Kessler, I., Koch, S. and Wenzel, T. Analysis of glycoproteins in human serum by means of glycospecific magnetic bead separation and LC-MALDI-TOF/TOF analysis with automated glycopeptide detection. *J. Biomol. Tech.* 2007, **18**: 252-258.

25. Xu, Y., Wu, Z., Zhang, L., Lu, H., Yang, P. and Webley, P.A. Highly specific enrichment of glycopeptides using boronic acid-functionalized mesoporous silica. *Anal. Chem.* 2008, **81**: 503-508. doi: 10.1021/ac801912t.

26. Alvarez-Manilla, G., Guo, Y., Warren, N.L., Orlando, R. and Pierce, M. Tools for glycoproteomic analysis: size exclusion chromatography facilitates identification of tryptic glycopeptides with N-linked glycosylation sites. *J. Proteome Res.* 2006, **5**: 701-708. doi: 10.1021/pr050275j.

27. Jia, W., Lu, Z., Fu, Y., Wang, H.P., Wang, L.H. and Chi, H. A strategy for precise and large scale identification of core fucosylated glycoproteins. *Mol. Cell Proteomics* 2009, **8**: 913-923. doi: 10.1074/mcp.M800504-MCP200.

28. Lewandrowski, U., Lohrig, K., Zahedi, R., Wolters, D. and Sickmann, A. Glycosylation site analysis of human platelets by electrostatic repulsion hydrophilic interaction chromatography. *Clin. Proteomics* 2008, **4**: 25-36.

29. Zhang, H., Guo, T., Li, X., Datta, A., Park, J.E. and Yang, J. Simultaneous characterization of glyco- and phosphoproteomes of mouse brain membrane proteome with electrostatic repulsion hydrophilic interaction chromatography. *Mol. Cell Proteomics* 2010, **9**: 635-647. doi: 10.1074/mcp.M900314-MCP200.

30. Tajiri, M., Yoshida, S. and Wada, Y. Differential analysis of site-specific glycans on plasma and cellular fibronectins: application of a hydrophilic affinity method for glycopeptide enrichment. *Glycobiology* 2005, **15**: 1332-1340. doi: 10.1093/glycob/cwj019.

31. Li, Y.L., Wu, J., Wei, D., Zhang, D.W., Feng, H. and Chen, Z.N. Newcastle disease virus represses the activation of human hepatic stellate cells and reverses the development of hepatic fibrosis in mice. *Liver Int.* 2009, **29**: 593–602. doi: 10.1111/j.1478-3231.2009.01971.x.

32. Qin, Y., Zhong, Y., Yang, G., Ma, T., Jia, L. and Huang, C. Profiling of concanavalin A-binding glycoproteins in human hepatic stellate cells activated with transforming growth factor-β1, *Molecules* 2014, **19**: 19845-19867. doi: 10.3390/molecules191219845.

33. Sun, S., Zhou, J.Y., Yang, W. and Zhang, H. Inhibition of protein carbamylation in urea solution using ammonium-containing buffers.

Anal. Biochem. 2014, **446**: 76–81. doi: 10.1016/j.ab.2013.10.024.
34. Sun, S., Zhao, F., Wang, Q., Zhong, Y., Cai, T., Wu, P., Yang, F. and Li, Z. Analysis of age and gender associated N-glycoproteome in human whole saliva. *Clin. Proteomics* 2014, **11**: 25. doi: 10.1186/1559-0275-11-25.
35. Palmisano, G., Melo-Braga, M.N., Engholm-Keller, K., Parker, B.L. and Larsen, M.R. Chemical deamidation: a common pitfall in large-scale N-linked glycoproteomic mass spectrometry-based analyses. *J. Proteome Res.* 2012, **11**: 1949–1957. doi: 10.1021/pr2011268.
36. Conesa, A., Götz, S., Garcia-Gomez, J.M., Terol, J., Talon, M. and Robles, M. Blast2GO: A universal tool for annotation, visualization and analysis in functional genomics research. *Bioinformatics* 2005, **21**: 3674–3676. doi: 10.1093/bioinformatics/bti610.
37. Ye, J., Fang, L., Zheng, H., Zhang, Y., Chen, J. and Zhang, Z. WEGO: A web tool for plotting GO annotations. *Nucl. Acids Res.* 2006, 34: W293–W297. doi: 10.1093/nar/gkl031.
38. Kanehisa, M., Goto, S., Sato, Y., Furumichi, M. and Tanabe, M. KEGG for integration and interpretation of large-scale molecular datasets. *Nucl. Acids Res.* 2012, 40: D109–D114. doi: 10.1007/978-1-62703-107-3_17.
39. Huang, D.W., Sherman, B.T. and Lempicki, R.A. Systematic and integrative analysis of large gene lists using DAVID Bioinformatics Resources. *Nat. Protoc.* 2009, **4**: 44–57. doi: 10.1038/nprot.2008.211.
40. Szklarczyk, D., Franceschini, A., Kuhn, M., Simonovic, M., Roth, A. and Minguez, P. The STRING database in 2011: Functional interaction networks of proteins, globally integrated and scored. *Nucl. Acids Res.* 2011, **39**: D561–D568. doi: 10.1093/nar/gkq973.
41. UniProt Consortium. The UniProt Consortium, Reorganizing the protein space at the Universal Protein Resource (UniProt). *Nucleic Acids Res.* 2012, **40**: D71-D75. doi: 10.1093/nar/gkr981.
42. Ott, C.M. and Lingappa, V.R. Integral membrane protein biosynthesis: why topology is hard to predict. *J. Cell Sci.* 2002, **115**: 2003−2009.
43. Roth, J. Protein N-glycosylation along the secretory pathway: Relationship to organelle topography and function, protein quality control, and cell interactions. *Chem. Rev.* 2002, **102**: 285−303. doi: 10.1021/cr000423j.
44. Spiro, R.G. Protein glycosylation: nature, distribution, enzymatic formation, and disease implications of glycopeptide bonds. *Glycobiology* 2002, 12: 43R−56R. doi: 10.1093/glycob/12.4.43R.
45. Gardinassi, L.G., Dotz, V., Hipgrave Ederveen, A., de Almeida, R.P., Nery Costa, C.H. and Costa, D.L. Clinical severity of visceral leishmaniasis is associated with changes in immunoglobulin g fc N-glycosylation. *MBio.* 2014, **5**: e01844. doi: 10.1128/mBio.01844-14.
46. Miyahara, K., Nouso, K., Dohi, C., Morimoto, Y., Kinugasa, H. and Wada, N. Alteration of N-glycan profiles in patients with chronic hepatitis and hepatocellular carcinoma. *Hepatol. Res.* 2014, doi: 10.1111/hepr.12441. [Epub ahead of print]
47. Zhu, J., Sun, Z., Cheng, K., Chen, R., Ye, M. and Xu, B. Comprehensive mapping of protein N-glycosylation in human liver by combining hydrophilic interaction chromatography and hydrazide chemistry. *J. Proteome Res.* 2014, **13**: 1713-1721. doi: 10.1021/pr401200h.
48. Lee, J.Y., Kim, J.Y., Cheon, M.H., Park, G.W., Ahn, Y.H., Moon, M.H. and Yoo, J.S. MRM validation of targeted nonglycosylated peptides from N-glycoprotein biomarkers using direct trypsin digestion of undepleted human plasma. *J. Proteomics* 2014, **98**: 206-217. doi: 10.1016/j.jprot.2014.01.003.
49. Blake, T.A., Williams, T.L., Pirkle, J.L. and Barr, J.R. Targeted N-linked glycosylation analysis of H5N1 influenza hemagglutinin by selective sample preparation and liquid chromatography/tandem mass spectrometry. *Anal. Chem.* 2009, **81**: 3109-2118. doi: 10.1021/ac900095h.
50. Fletcher, D.A. and Mullins, R.D. Cell mechanics and the cytoskeleton. *Nature* 2010, **463**: 485–492. doi: 10.1038/nature08908.
51. Chen, C.S., Alonso, J.L., Ostuni, E., Whitesides, G.M. and Ingber, D.E. Cell shape provides global control of focal adhesion assembly. *Biochem. Bioph. Res. Co.* 2003, **307**: 355–361. doi: 10.1016/S0006-291X(03)01165-3.
52. Weiskirchen, R. and Tacke, F. Cellular and molecular functions of hepatic stellate cells in inflammatory responses and liver immunolog. *Hepatobiliary Surg. Nutr.* 2014, **3**: 344-363. doi: 10.3978/j.issn.2304-3881.2014.11.03.
53. Rockey, D.C., Boyles, J.K. and Gabbiani, G. Rat hepatic lipocytes express smooth muscle actin upon activation in vivo and in culture. *J. Submicrosc. Cytol. Pathol.* 1992, **24**: 193–203.
54. Saab, S., Tam, S.P. and Tran, B.N. Myosin mediates contractile force generation by hepatic stellate cells in response to endothelin-1. *J. Biomed. Sci.* 2002, **9**: 607–612. Doi: 10.1007/BF02254988.
55. Yee, H.F. Ca^{2+} and rho signaling pathways: two paths to hepatic stellate cell contraction. *Hepatology* 2001, **33**: 1007–1008. doi: 10.1053/jhep.2001.23901.
56. Laleman, W., Van Landeghem, L. and Severi, T. Both Ca^{2+}-dependent and -independent pathways are involved in rat hepatic stellate cell contraction and intrahepatic hyperresponsiveness to methoxamine. *Am. J. Physiol. Gastrointest. Liver Physiol.* 2007, **292**: G556–G564. doi: 10.1152/ajpgi.00196.2006.
57. Lortat-Jacob, H. The molecular basis and functional implications of chemokine interactions with heparan sulphate. *Curr. Opin. Struct. Biol.* 2009, **19**: 543-548. doi: 10.1016/j.sbi.2009.09.003.
58. Lin, X. Functions of heparan sulfate proteoglycans in cell signaling during development. *Development* 2004, ***131***: 6009-6021. doi: 10.1242/dev.01522.
59. Rosse, C. Linch, M. Kermorgant, S. Cameron, A.J. Boeckeler, K. and Parker, P.J. PKC and the control of localized signal dynamics. *Nat. Rev. Mol. Cell Biol.* 2010, **11**: 103-112. doi: 10.1038/nrm2847.